

2. Hwang, K. J.; Park, K. H. *U.S. Pat.* 5,389,667.
3. Lee, L. F.; Schleppek, F. M.; Schneider, R. W.; Campbell, J. W. *J. Heterocyclic Chem.* **1990**, *27*, 243.
4. Moedritzer, K.; Rogers, M. D. *U.S. Pat.* 4,964,895.
5. Lee, L. F.; Moedritzer, K.; Rogers, M. D. *U.S. Pat.* 4,855,442.
6. Gaede, B. J.; Torrence, L. L. *U.S. Pat.* 4,984,902.
7. Hamper, B. C. *J. Fluorine Chem.* **1990**, *49*, 23.
8. Hamper, B. C.; Kurtzweil, M. L.; Beck, J. P. *J. Org. Chem.* **1992**, *57*, 5680.
9. (a) Chapman, A. W. *J. Chem. Soc.* **1925**, 127, 1992. (b) March, J. *Advanced Organic Chemistry*, 4th Ed.; John Wiley & Sons: New York, 1992; p 1155.
10. DeStevens, G.; Halamandaris, A.; Wenk, P.; Dorfman, L. *J. Am. Chem. Soc.* **1959**, *81*, 6292.

Dynamics of OH Photodissociation above the Threshold to O(¹D): A Quantum Mechanical Analysis

Sungyul Lee

Department of Chemistry,
College of Natural Sciences, Kyunghee University,
Kyungki-do 449-701, Korea

Received June 13, 1995

Diatomic photodissociation processes are very important in molecular reaction dynamics for several reasons. *Ab initio* results on the potential energy curves, transition dipole moments and nonadiabatic interactions of many diatomic molecules are available for detailed dynamic calculations. The theory of photodissociation¹ is well developed so that direct comparison between theoretical calculations and experiments are now possible. Developments of powerful experimental methods such as multiphoton technique has made it possible to probe the dynamic processes of molecules at wide ranges of excitation energy.

In a series of papers,²⁻⁸ we have shown that the exact treatments of the photodissociation processes are very useful for elucidating many interesting dynamic behaviors of molecules. It has been demonstrated that nonadiabatic interactions both in the Franck-Condon region and in asymptotic region can significantly affect such important dynamic observables as the shape of the resonances,^{2,4-6} product branching ratios⁴⁻⁶ and angular distributions.^{7,8} The magnitude of these influences has been found to be large at energies below the threshold to O(¹D) in the photodissociation of OH molecule. Crossings between the bound $A^2\Sigma^+$ and the repulsive $^4\Sigma^-$, $^2\Sigma^-$ and $^4\Pi$ states result in well-known predissociation in this energy regime, and quantum interference between the indirect dissociation pathway via $A^2\Sigma^+$ state and the direct dissociation pathway through $^2\Sigma^-$ state has been predicted^{2,4-6} to give rise to asymmetric resonances in the photodissociation cross sections. It has also been shown that

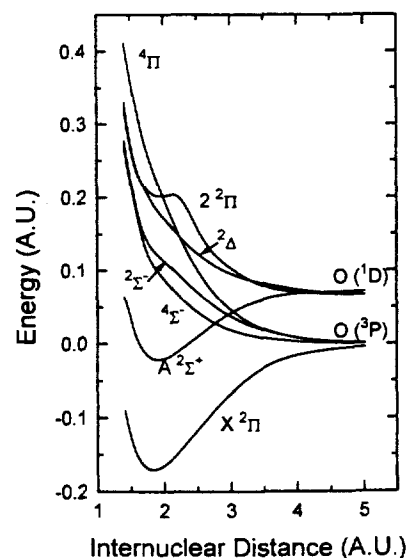


Figure 1. Potential curves of OH.

the branching ratios of O(³P, $j=0, 1, 2$) exhibit rapid variations near these asymmetric resonances.⁴⁻⁶ Implications of this latter finding have been discussed in the spirit of coherent control of dynamic processes.

Above the dissociation threshold to O(¹D), all of the potential curves (including $A^2\Sigma^+$) are dissociative (see Figure 1), and the dissociation is direct in this energy regime. It is well known⁹ that the direct dissociation processes approach a diabatic limit at high kinetic energies of the photofragments, which are characterized by energy independent product branching ratios and angular distributions. Actually, it is in this high energy regime that particular values of the observables can be correlated with the symmetries of the excited states and dissociation pathways in a simple fashion.^{9,10} We demonstrate in this work that dissociations to O(³P) fragments show signs of diabatic limit behaviors at energies above the threshold to O(¹D). However, dissociation processes to O(¹D) exhibit very different patterns, characterized by highly oscillating fragment anisotropy parameters, as a result of the quantum interference between two direct dissociating pathways.

The theory has been described in detail elsewhere,⁶ and we only give a brief summary in this paper. Since the two oxygen atomic term limits, O(³P) and O(¹D), are involved in OH photodissociation (see Figure 1), we construct two transformation matrices,^{6,9} each of which describes the connections between an atomic term and adiabatic Born-Oppenheimer states correlating with it. Two kinds of basis functions are employed in the calculations to evaluate the total Hamiltonian. Hund's case (a) basis function of parity p , $|JM\Lambda\Sigma p\rangle$ is employed to evaluate the electronic Hamiltonian, which is diagonal in this basis. J is the total angular momentum, M is its component along the space-fixed axis, S is the total spin, Λ and Σ are the components of J and S along the molecular axis, respectively, and C denotes any other electronic state labels. The asymptotic basis functions $|JMj_l j_H\rangle$ are used to evaluate the spin-orbit Hamiltonian and the rotational part $l(l+1)/2\mu r^2$, since they are diagonal in these basis functions. Here j_o (j_H) are the total electronic

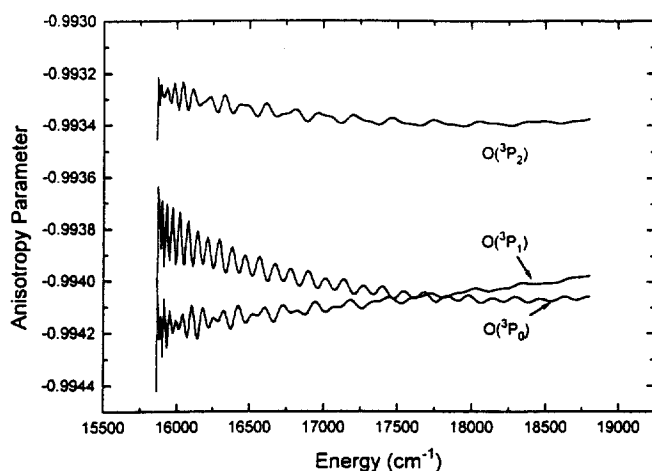


Figure 2. Anisotropy parameters for $O(^3P)$. The initial ground state is the $X^2\Pi^+_{3/2}$ state ($J_i=3/2$ and $v_i=0$). The zero of energy is defined as the statistical average of the energies of $O(^3P, j=0, 1, 2)$.

angular momentum of the oxygen (hydrogen) fragment and l is the orbital angular momentum, $j=j_o+j_H$, and C_o denotes extra quantum numbers needed to describe the electronic states of oxygen besides j_o (that is, spin and electronic orbital angular momentum quantum number). The two basis functions are related to each other by r -independent transformation matrices $\langle j_l C_{o j_H} | C A S \Sigma p \rangle_j$. Close-coupled equations are solved for the multichannel continuum wavefunction (14×14 matrix) of good parity. The continuum wavefunction is propagated in the adiabatic Born-Oppenheimer (ABO) basis $|J M C A S \Sigma p \rangle$ using the Renormalized Numerov method.¹¹ The transition amplitudes in ABO basis are transformed into the asymptotic basis $|J M j_l C_{o j_H} \rangle$ by the two frame transformation matrices at the end of the propagation and appropriate boundary conditions are imposed. The transition amplitudes for dissociation to a specific fine structure component of the oxygen atom is calculated by employing the Golden Rule. Cooley's method¹² is used to evaluate the initial bound state vibrational wave function of the $X^2\Pi$ state.

Figure 1 depicts the potential curves of OH. Above the dissociation limit to $O(^1D)$, the photodissociation is direct. Nonadiabatic (spin-orbit and Coriolis) couplings among electronic states correlating to $O(^3P)$ term limit are very small compared with the kinetic energies of the $O(^3P)$ fragments, and their effects on the dissociations to $O(^3P)$ are expected to be minimal. Figure 2 shows that the anisotropy parameters for $O(^3P, j=0, 1, 2)$ are nearly energy independent, and are very close to -1 , which is the diabatic limit value⁹ for excitations from $^2\Pi$ to $^2\Sigma$ state. This is consistent with our previous demonstration⁶ that the branching ratios to $O(^3P, j=0, 1, 2)$ states are very similar to the diabatic limit values (0.111 : 0.333 : 0.555) in this energy regime. The small amplitude variations of the anisotropy parameters indicate that the effects of the nonadiabatic interactions still persist in this high energy regime. For dissociations to $O(^1D)$, however, the situation is quite different. The kinetic energy of the $O(^1D)$ fragments is not very large in this energy regime, and the effects of the nonadiabatic (spin-orbit and Coriolis) interactions between the two dissociative $^2\Delta$ and $^2\Pi$ states

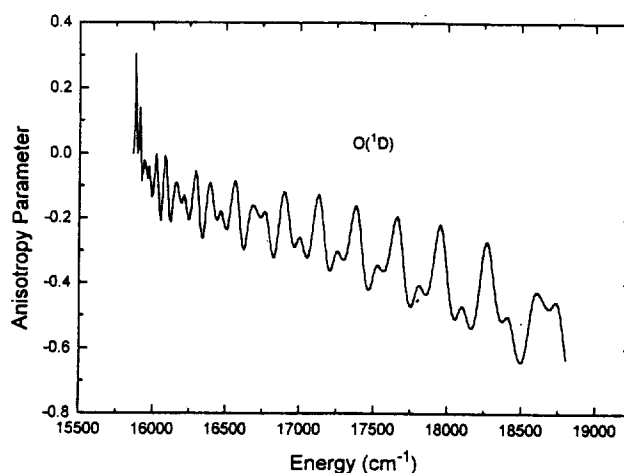


Figure 3. Anisotropy parameters for $O(^1D)$. The initial ground state is the $X^2\Pi^+_{3/2}$ state ($J_i=3/2$ and $v_i=0$). The zero of energy is defined as the statistical average of the energies of $O(^3P, j=0, 1, 2)$.

are expected to be significant. Since both of the $^2\Delta$ and $^2\Pi$ states are optically connected with the ground $X^2\Pi$ state, quantum interference between these two dissociation channels may affect the dissociation processes to $O(^1D)$. Figure 3 clearly shows the influence of the quantum interference on the angular distributions. The anisotropy parameter for $O(^1D)$ exhibits highly oscillatory variation as a function of the excitation energy.

Dissociations of OH considered in this work are those resulting from excitations of the $X^2\Pi^+_{3/2}$ lambda doublet component (with $J_i=3/2$ and $v_i=0$). Selective production of the lambda doublets ($X^2\Pi^+_{3/2}$ and $X^2\Pi^-_{3/2}$), which are separated by only 0.05 cm^{-1} , has recently been achieved by Schreel *et al.*,¹³ employing the hexapole selector in a molecular beam experiment. In order to measure the product branching ratios and the angular distributions, and to investigate the effects of the nonadiabatic interactions on these observables, however, the lambda doublet components need not be separated, since the two components are of different symmetry, and the coherent excitations of the two lambda doublet components do *not* lead to quantum mechanical interference. We have performed quantum mechanical calculations for photodissociations resulting from the coherent excitations of the two lambda doublet components, and found that the results are identical to the incoherent processes. We are currently investigating the influence of the quantum interferences on the fluorescence anisotropy parameters.

Acknowledgment. This work has been supported by the Korea Science and Engineering Foundation.

References

- Schinke, R. *Photodissociation dynamics*; (Cambridge University Press: Cambridge, 1993).
- (a) Kim, B.; Yoshihara, K.; Lee, S. *Phys. Rev. Lett.* **1994**, *73*, 424. (b) Lee, S. *Bull. Kor. Chem. Soc.* **1995**, *16*, 387.
- (a) Lee, S.; Park, C. R.; Kim, H. L.; Park, S. C. *Chem. Phys. Lett.* **1995**, *233*, 207. (b) Lee, S. *Bull. Kor. Chem. Soc.* **1995**, *16*, 449.

4. Lee, S. *Chem. Phys. Lett.* **1995**, *240*, 595.
5. Lee, S. *J. Phys. Chem.* (in press).
6. Lee, S. *J. Chem. Phys.* **1995**, *103*, 3501.
7. (a) Lee, S. *Chem. Phys. Lett.* **1995**, *243*, 250.
8. Lee, S. (Submitted for publication).
9. Singer, S. J.; Freed, K. F.; Band, Y. B. *Adv. Chem. Phys.* **1985**, *61*, 1.
10. Greene, C. H.; Zare, R. N. *Ann. Rev. Phys. Chem.* **1982**, *33*, 119.
11. Johnson, B. R. *J. Chem. Phys.* **1977**, *67*, 4086.
12. Cooley, J. W. *Math. Comp.* **1961**, *383*, 15.
13. Schreel, K.; Schleipen, J.; Eppink, A.; ter Meulen, J. J. *J. Chem. Phys.* **1993**, *99*, 8713.

Synthesis and Hydrogenation Reaction of Iridium Complexes Containing L-Methionine Methyl Ester

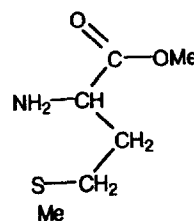
Young-ae W. Park* and Ji Hyang Kim

Department of Chemistry,
Sang Myung Women's University,
Seoul 110-743, Korea

Received June 21, 1995

Chemistry of transition metal complexes of sulfur-containing amino acid ligands such as *l*-cysteine, *l*-cysteine methyl ester and *l*-methionine has been studied due to the biological significance of the interaction between metal ion and sulfur-containing amino-acids.¹⁻¹⁰ Those ligands can chelate through -NH₂ and carbonyl, -NH₂ and sulfur, or all of three sites. Amino acids exist in living systems in one enantiomeric form predominantly, since nature prefers for a particular enantiomer which complements the life. Reactions of transition metals with asymmetric ligands can lead to the catalysis for asymmetric hydrogenation. Although various complexes of sulfur containing amino acids have been prepared, iridium(I) complexes of those ligands have not been made. We report herein the synthesis and hydrogenation reactions of iridium complexes containing *l*-methionine methyl ester (MME) li-

gand to investigate the coordination sites of MME as well as the possibility as catalysts.



MME

Synthesis. The reaction of [IrCl(COD)]₂ (COD=1,5-cyclooctadiene) with MME·HCl by 1:2 mole ratio of Ir to MME ligand in the mixture of methanol and ether at 25 °C gives a yellow crystalline product (**1**). The absorption bands at 1744 cm⁻¹ and 3190 cm⁻¹ in the IR spectrum of **1** are assigned to the uncoordinated carbonyl group of the ester and the coordinated amine respectively, indicating the MME ligand is bonded through amine and sulfur. In the free MME ligand, ν_{CO} is found at 1744 cm⁻¹, however, ν_{NH₂} can not be observed since the ligand exists as the ammonium salt (ν_{RNH₂⁺} is found as strong multiple bands at 2720, 2614 and 2510 cm⁻¹). The uncoordinated NH₂ is observed in the range of 3300-3450 cm⁻¹, while the coordinated NH₂ is observed in the range of 3000-3200 cm⁻¹ in the literature.⁵⁻⁸ The bands for Ir-N at 528 cm⁻¹ and Ir-S at 361 cm⁻¹ also confirm the ligand is coordinated through amine and sulfur.⁴⁻¹¹ The ¹H NMR spectral data of the complexes in this work are shown in Table 1. Comparing with the free MME ligand, the resonance of the S-CH₃ in **1** is slightly shifted downfield by 0.10 ppm on coordination of sulfur to iridium. Elemental analyses of all the complexes of this work are listed in Table 2 and the data indicates two MME ligands are included in the complex **1** and the electrical conductivity in methanol is 92 cm²ohm⁻¹mol⁻¹, which is typical of 1:1 electrolytes in methanol.¹² Thus, the chloride is anionic and the molecular formula of the complex is considered to be Ir[MME]₂Cl (**1**). The molecular structure can be **1a** with two MME ligands being trans to each other or **1b** with cis configuration, but **1a** may be more probable due to the steric hindrance of both S-methyl groups on the same side in **1b**. The reaction of [IrCl(COE)]₂ (COE=cyclooctene) with MME by 1:2 mole ratio in the presence of NaAsF₆ produces a yellow compound (**2**). The IR spectrum of **2** shows a band

Table 1. Characteristic ¹H NMR Spectral Data of the Complexes^a

Compound	S-CH ₃	O-CH ₃	-CH ₂	S-CH ₂	-NH ₂	-CH	-CH
1	2.25, s	3.87, s	2.30-2.40, m	2.70, t	3.30, s	4.30, t	
2^c	2.23, s	3.80, s	1.80-2.80, m	b	3.30, s	4.20, t	5.32, t
3^{c,d}	2.25, s	3.83, s	2.30-2.40, m	b	3.35, s	4.30, t	5.62, t
			(MME)				
			[1.50-1.80, m				
			2.60-2.80, m				
			(COE)				

^as, singlet; t, triplet; m, multiplet. ^b not separately found due to the multiplet of -CH₂. ^c water peak; δ 4.80 ppm, s. ^d triphenylphosphine; δ 7.20-7.80 ppm.